Journal of Advanced Engineering Research
ISSN: 2393-8447
Volume 3, Issue 1, 2016, pp.56-60

Effect of Ball size on the Characterization of Mg-Zn-Ca alloy Prepared by Mechanical Alloying

M. Thirumurugan[1,*], C. Aguilar[2], D. Guzman[3]

[1]Department of Mechanical Engineering, B.S. Abdur Rahman University, Chennai-48, India.
[2]Department of Metallurgical and Materials Engineering, University Santa Maria, Chile.
[3]Department of Metallurgical Engineering, Universidad de Atacama, Copiapo, Chile.

*Corresponding author email: thirumurugan@bsauniv.ac.in, Tel.: +91 44 22751347

ABSTRACT

Mechanical alloying is one of the important techniques used to produce the homogeneous alloys and amorphous materials. This paper investigates the effects of different ball sizes to achieve the amorphous phase in Mg-Zn-Ca ($Mg_{66}Zn_{30}Ca_4$) alloy system through the mechanical alloying technique. The compositions of $Mg_{66}Zn_{30}Ca_4$ (at.%) powders are synthesized by using the mechanical alloying for 10 hours in a planetary mill with 10:1 BPR (ball to powder ratio). The two different diameters of ball 6mm and 15mm are used in this dry milling process. It has shown that the 15mm balls produce the good broadened diffracted (halo) peaks than the 6mm balls. The 6mm balls produce more nano (88.82nm) sized crystalline peaks than the 15mm balls.

Keywords - Amorphization, Ball size, Dry milling, Magnesium alloy, Mechanical Alloying

1. INTRODUCTION

Magnesium (Mg) alloys and magnesium based amorphous materials offer exceptional properties in constructional and bio-medical applications than the conventional metallic materials. Due to the poor creep and corrosion resistance of Mg alloys, it is necessary to develop the new Mg alloys by combining the different alloying elements [1, 2]. The element of calcium (Ca) is added to the Mg alloys to improve the creep resistance effectively [3]. Similarly zinc (Zn) is added to the magnesium alloys to increase hardness by solid solution hardening [4, 5]. Combined Mg-Zn-Ca metallic glass (MG) materials are found as biocompatible, because the release of hydrogen is significantly reduced by zinc and oxygen-rich passivating layer [6-8]. Many techniques are available for producing alloys and amorphous materials, but the mechanical alloying (MA) is one of effective method [9]. In ball milling, the grinding balls are transferred high-energy to the powders by collision. Also the grinding balls produce a severe plastic deformation in the milled powders (elemental or alloy). During deformation, the powder particles are fractured and welded by the grinding media (contains grinding balls and PCA) and produces the homogeneous microstructures. Normally in high energy milling, the crystal sizes are decreased to some critical values. More and more of energy supplied to these crystals and energy accumulation in the volume or at the surface of crystals causes further deformation of crystals, subsequently it leads to amorphization [10]. To form the amorphization quickly, the alloy systems must satisfy the following three empirical rules: (1) system consists of more than three elements (multi-component); (2) significant difference in atomic size ratios above (about12% or more) among the constituent elements; and (3) negative heat of mixing among the constituent elements [11]. There are several variables like ball size, ball and vial material, ball to powder ratio, milling time, milling environment and temperature rise are involved in the milling process which may affect the characteristics of milling [12]. To produce an amorphous powder effectively it is very much important to control these milling variables. Presence information about the physical metallurgy of Mg-Ca-Zn alloys is complicated to understand and unclear. This work aims to understand the effects of ball size in amorphization of ($Mg_{66}Zn_{30}Ca_4$) Mg-Zn-Ca alloy for a specified milling time. And this information introduces the knowledge to produce the metallic glasses through mechanical milling/alloying technique.

2. EXPERIMENTAL PROCEDURE

Elemental powders of Mg (99.9%, -50 mesh), Zn (99.9%, < 5μm), and Ca (99.9%, -8 mm to3.25 mm), were weighed to yield the desired composition of

$Mg_{66}Zn_{30}Ca_4$. The weighed powders took in the 250 ml high speed steel vial together with high carbon steel balls in argon-filled glove box equipment. Two different diameters of balls (15 and 6 mm) were used in this milling process to understand their effects in producing the amorphous phases. Intentionally, no addition of process control agent (PCA) was employed in this process. The ball to powder ratio was maintained as 10:1. The Planetary ball mill (PM-400) was employed for the mechanical alloying. The planetary ball mill was operated by the following program: 10 min-OFF and 10 min-ON, speed: 300 rpm, Directions: reverse and forward. The powders were milled for 10 hours. After milling the powders were carefully removed from the vial and balls. The SEM, XRD and DSC analyses were performed on the powder samples. SEM analysis was performed to understand the particle size and morphology of milled powders. SEM-EDS (Energy Dispersive Spectrum) analysis was used to find out the influence of alloying elements in the milled powders by quantitatively. XRD characterization was used to verify the amorphous state and to check the formation intermetallic phases with respect to the ball sizes. The XRD patterns were obtained using PANalytical X'pert Pro powder X-ray diffractometer with a CuK_α radiation. The XRD spectrum was acquired from 20°to 120° 2θ with a 0.02° step size and 7s of scan time. All the obtained X-ray patterns were analyzed using X'Pert HighScore Plus software. The thermal transformations, thermal stability, glass transition and crystallization temperatures were studied by means of calibrated non-isothermal DSC Instrument under a continuous flow rate of (50.00 ml/min) purified nitrogen. Samples were placed in an alumina crucible and covered with a lid before starting thermal analysis. The samples were heated at rates of 10°C/min subsequently cooled to room temperature at a constant cooling rate of 10°C/min.

3. RESULTS AND DISCUSSIONS

Fig. 1 shows the SEM images of Mg, Zn, Ca powders used in the milling process. The Mg and Ca powders exhibit the micron sized particles with irregular morphologies. The Zn powder shows finer particles with spherical morphology.

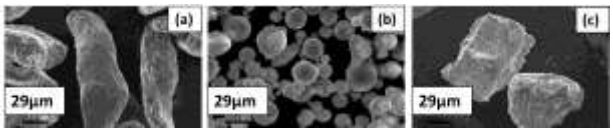

Fig. 1 SEM images of (a) Mg (b) Zn (c) Ca powders- As received condition

Normally in the ball milling process, different techniques are adopted to reduce the cold welding to promote fracturing. By adding the suitable process control agent (stearic acid or hydrocarbons) to the constituent powders employed in the milling process, contributes to perfect metal to metal contact which is necessary to avoid cold welding phenomenon. But in this work, intentionally no PCA is added and the powders were dry milled in an argon environment. Whenever two grinding balls start colliding in the milling process, a small amount of powder is trapped and collided/fractured in between them. In this process, different powder morphology is obtained due to the absence of PCA. For the soft powders like magnesium, the powder particles were flattened as layers due to the cold welding. This generates the formation of layered, powder particles around the vial and balls. The layer consist the ingredients of starting powders. Fig. 2 shows the images of balls and vials after 10 hours of milling. The macroscopic image clearly shows the sticking of powder particles in and around the balls and vials. The 6mm diameter of ball outer surfaces is completely enclosed by the powder particles whereas 15 mm diameter ball surfaces are less enclosed.

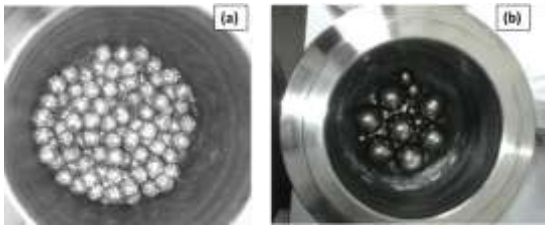

Fig. 2 Macroscopic images of vial and two different diameters of balls used in milling (a) 6 mm (b) 15 mm.

Fig. 3 shows the SEM images of $Mg_{66}Zn_{30}Ca_4$ powders milled for 10 hrs. The milled powders exhibit an agglomerated particle. Due to the agglomeration effect, the milled powder particles are enlarged which makes difficult to measure the particle size of the powder from the SEM images. The SEM-EDS analysis, results that the milled particles contain oxygen and iron as contamination. The atomic percentile values of individual elements (Mg, Zn and Ca) in the milled powders are less when compared to the atomic percentile values of as mixed powders, which indicates the formation of intermetallic phases among the constituent elements.

Fig. 4 shows the XRD patterns of Mg, Zn and Ca elemental powders used in the milling process. There are no new peaks were found other than the peaks of individual elements.

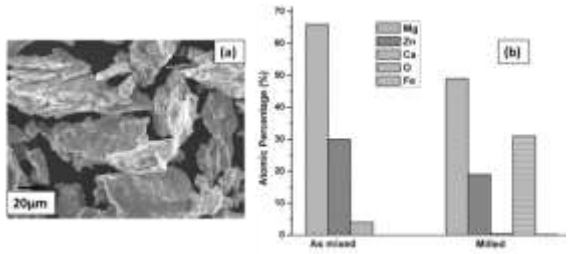

Fig. 3 SEM images of ball milled $Mg_{66}Zn_3Ca_4$ powders - 10 h (b) EDS distribution chart

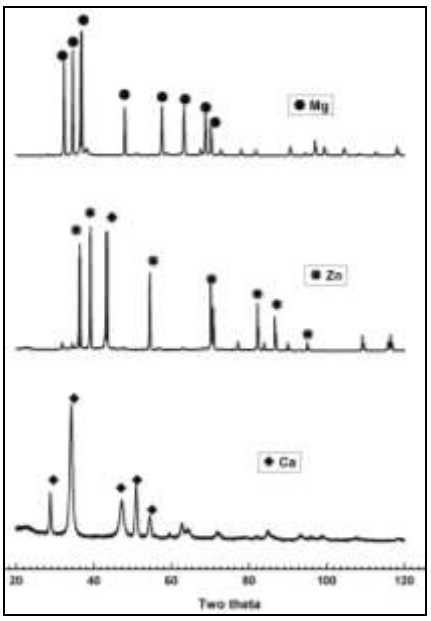

Fig. 4 X-ray patterns of Mg, Zn and Ca powders –As received condition

As per the thermodynamic calculations and ternary phase diagrams of the Mg-Zn-Ca system, consists of four solution phases (fcc, hcp and bcc terminal solid solutions, and liquid), fourteen binary compounds (Ca_3Zn, Ca_5Zn_3, CaZn, $CaZn_2$, $CaZn_3$, $CaZn_5$, $CaZn_{11}$, $CaZn_{13}$, $CaMg_2$, $MgZn_2$, Mg_2Zn_{11}, Mg_2Zn_3, Mg_7Zn_3 and MgZn) and one ternary compound ($Ca_2Mg_6Zn_3$/$Ca_2Mg_5Zn_{13}$) [13-19]. Since the milled powder particle contains the oxygen and iron as contamination, the reflections of MgO, ZnO, CaO and Fe are included in the XRD peaks indexing. Fig. 5 shows the X-ray patterns of $Mg_{66}Zn_{30}Ca_4$ powders milled by different ball sizes. The 10 hours milled $Mg_{66}Zn_{30}Ca_4$ powders reveals different phases/compounds for different ball sizes. Both the milled powders reveal broad diffracted (amorphous like halo regime) and crystalline peaks. The powders milled using 15mm balls shows a very broad diffracted peak (2θ range from 28° to 50°) with less intensity crystalline peaks. But the powders milled using 6mm balls shows a broad diffracted peak (2θ range from 34° to 48°) with high intensity crystalline peaks because of small ball size. The 6mm balls transfers more energy to the powders during milling results better amorphization. However, the presence of crystalline peaks and broad diffracted peaks indicates the coexistence of crystalline and amorphous phases.

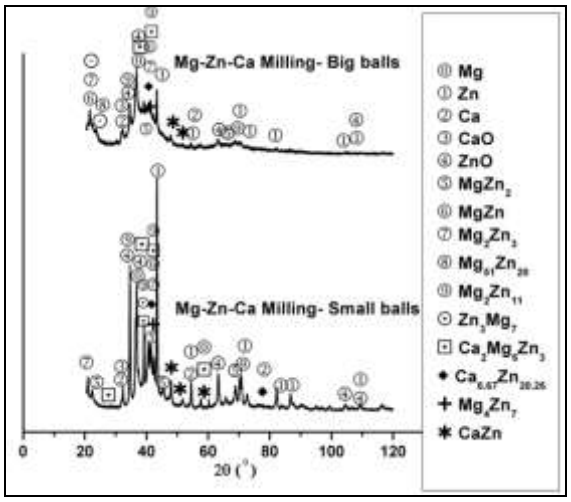

Fig. 5 XRD patterns of $Mg_{66}Zn_{30}Ca_4$powders milled for 10 hours using different diameters of ball 6mm (bottom) and 15 mm (top)

Mg_2Zn_3, Mg_2Zn_{11}, CaZn, Zn, ZnO and $Ca_2Mg_6Zn_3$phases were mostly present in both kinds of milling. The phases were identified using the X´Pert high score plus software which contains the reflections of all phases in Mg-Zn-Ca [20]. Depends on the amount of Mg, Zn and Ca are mixing or trapping between the grinding balls, the formations of intermetallic phases varies with respect to the ball sizes. The crystallite size has been calculated by using the Scherrer formula/calculations. The crystallite size of powder milled using 15mm (big) balls are calculated as 55.5nm whereas the crystallite size of powder milled using 6mm (small) balls is calculated as 88.82nm. The small sized ball produces more nano-sized particles than big balls. Fig. 6 shows the DSC plot of Mg, Zn and Ca elements. There are no thermal transformations in the samples of Mg and Ca. But Zn shows one shallow transformation (endothermic reaction) around 275°C which may possibly due to the contamination of zinc powders.

Fig. 7 shows the DSC analysis of $Mg_{66}Zn_{30}Ca_4$ powders milled for 10 hours. Both kinds of milled powders (milling using 6mm and 15mm balls) reveal an identical DSC transformation. Two endothermic peaks are revealed at 335°C (E1) and 350°C (E2), which may similar with the previous studies reported for Mg-Zn-Ca

system [21]. The first endothermic peak is related to the melting onset of some metastable phases, such as Mg_2Zn_3 with a lower melting point. Meanwhile, the second endothermic peak may be related to the dissolution of some stable precipitates such as $MgZn_2$ or $Ca_2Mg_6Zn_3$.

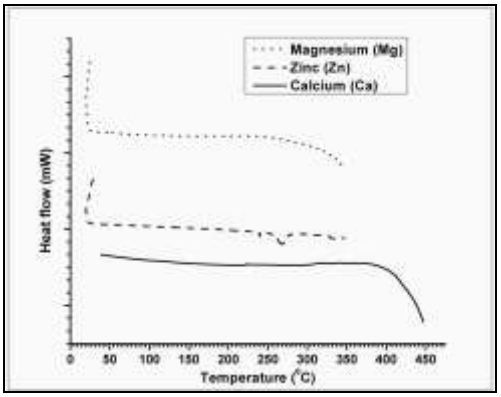

Fig. 6 DSC plots of Mg, Zn and Ca elements

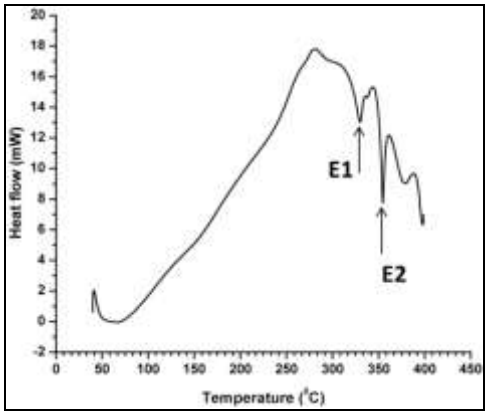

Fig. 7 DSC analysis of milled $Mg_{66}Zn_{30}Ca_4$ powders

4. CONCLUSIONS

The milled powders revealed that the powders were coated around the balls and vials. The oxygen contamination and the intermetallic phases of Mg-Zn-Ca composition were observed from SEM-EDS results. The powders milled with different ball size revealed the amorphous and crystalline peaks. The 15mm diameter balls resulted as broadened amorphous range, whereas the 6mm diameter balls revealed nano-sized intermetallic phases. The DSC results of the milled Mg-Zn-Ca system showed two endothermic peaks with shallow glass transition point.

5. ACKNOWLEDGEMENT

The authors would like to thank the financial support provided by FONDECYT project No: 3130471.

REFERENCES

[1] E. Pellicer, S. Gonzalez, A. Blanquer, S. Surinach, M.D. Baro, L. Barrios, On the biodegradability, mechanical behavior, and cytocompatibility of amorphous $Mg_{72}Zn_{23}Ca_5$ and crystalline $Mg_{70}Zn_{23}Ca_5Pd_2$ alloys as temporary implant material, *Journal of Biomed. Mater. Res. Part A, 101(2),* 2013, 502–517.

[2] A. Roy, D. Hong, J.P. Leonard, P.N. Kumta, Microstructure of Mg–Zn–Ca thin film derived by pulsed laser deposition, *Materials Science and Engineering B, 176(20),* 2011, 1690-1694.

[3] P. Yin, N.F. Li, T. Lei, L. Liu, C. Ouyan, Effects of Ca on microstructure, mechanical and corrosion properties and biocompatibility of Mg–Zn–Ca alloys, *Journal of Mater Sci: Mater Med., 24(6),* 2013, 1365-1373.

[4] R.J. Chadwick, The constitution of the alloys of magnesium and zinc, *Journal of the Institute of Metals, 449,* 1928, 285–299.

[5] E.D.R WHume-Rothery, The system magnesium–zinc. *Journal of the Institute of Metals, 41,* 1929, 119-138.

[6] B. Zberg, P.J. Uggowitzer, J.F. Loffler, MgZnCa glasses without clinically observable hydrogen evolution for biodegradable implants, *Nat Mater, 8,* 2009, 887-891.

[7] B. Zberg, E.R. Arata, P.J. Uggowitzer, J.F. Loffler, Tensile properties of glassy MgZnCa wires and reliability analysis using Weibull statistics, *Acta Mater, 57(11),* 2009, 32-23.

[8] X.N. Gu, Y.F. Zheng, S.P. Zhong, T.F. Xi, J.Q. Wang, W.H. Wang, Corrosion of, and cellular responses to Mg–Zn–Ca bulk metallic glasses, *Biomaterials, 31(6),* 2010, 1093-1103.

[9] M.K. Datta, D. Chou, D. Hong, P. Saha, S.J. Chung, B. Lee, Structure and thermal stability of biodegradable Mg–Zn–Ca based amorphous alloys synthesized by mechanical alloying, *Materials Science and Engineering B, 176(20),* 2011, 1637-1643.

[10] M.R. Vaezi, S.H.M. Shah Ghassemi, A. Shokuhfa, Effect of different sizes of balls on crystalline size, strain, and atomic diffusion on Cu-Fe nanocrystals produced by mechanical alloying, *Journal of Theoretical and Applied Physics, 6,* 2012, 29.

[11] A. Inoue, Stabilization of Metallic Super cooled Liquid and Bulk Amorphous Alloys, *Acta mater., 48(1),* 2000, 279-306.

[12] M. Ramezani, T. Neitzert, Mechanical milling of aluminum powder using planetary ball milling process, *Journal of Achievements in Materials and Manufacturing Engineering, 55(2),* 2012, 790-798.

[13] J. Clark, F. Rhins, Central Region of the Mg-Zn Phase Diagram, *Journal of Metals, 9,* 1957, 425-430.

[14] J.B Clark, L. Zabdyr, Z. Moser, Mg-Zn (Magnesium-zinc), Phase Diagrams of Binary, Magnesium Alloys, *ASM International, Metals Park,* 1988, 353-364.

[15] P.J. Spencer, A.D. Pelton, Y.B. Kang, P. Chartrand, C.D. Fuerst, Thermodynamic assessment of the Ca–Zn, Sr–Zn, Y–Zn and Ce–Zn systems, *Computer Coupling of Phase Diagrams and Thermochemistry. 32(2),* 2008, 423-431.

[16] M. Aljarrah, M. Medraj, Thermodynamic modelling of the Mg–Ca, Mg–Sr, Ca–Sr and Mg–Ca–Srsystems using the modified quasi chemical model, *Computer Coupling of Phase Diagrams and Thermochemistry, 32(2),* 2008, 240-251.

[17] C. Niu, M. Liu, C. Li, Z. Du, C. Guo, Thermodynamic description on the miscibility gap of the Mg-based solid solution in the Mg–Zn, Mg–Nd and Mg–Zn–Nd systems, CALPHAD: *Computer Coupling of Phase Diagrams and Thermochemistry, 34(4),* 2010, 428-433.

[18] P. Ghosh, M. Mezbahul-Islam, M. Medraj, Critical assessment and thermodynamic modeling of Mg–Zn, Mg–Sn, Sn–Zn andMg–Sn–Zn systems, CALPHAD: *Computer Coupling of Phase Diagrams and Thermochemistry, 36,* 2012, 28-43.

[19] Z. Yang, D. Shi, B. Wen, R. Melnik, Structural, elastic, electronic properties and heats of formation of Ca–Zn intermetallics from first principles calculations, *Journal of Alloys and Compounds, 524,* 2012, 53-58.

[20] PANalytical: XPert Highscore Plus V2.2a, (http://www.panalytical.com/index.cfm)

[21] Z. Tao, C. Ding, C. Zhen-hua, Microstructures and properties of rapidly solidified Mg-Zn-Ca alloys, Trans. *Nonferrous Met. Soc. China, 18(1),* 2008, 101-106.